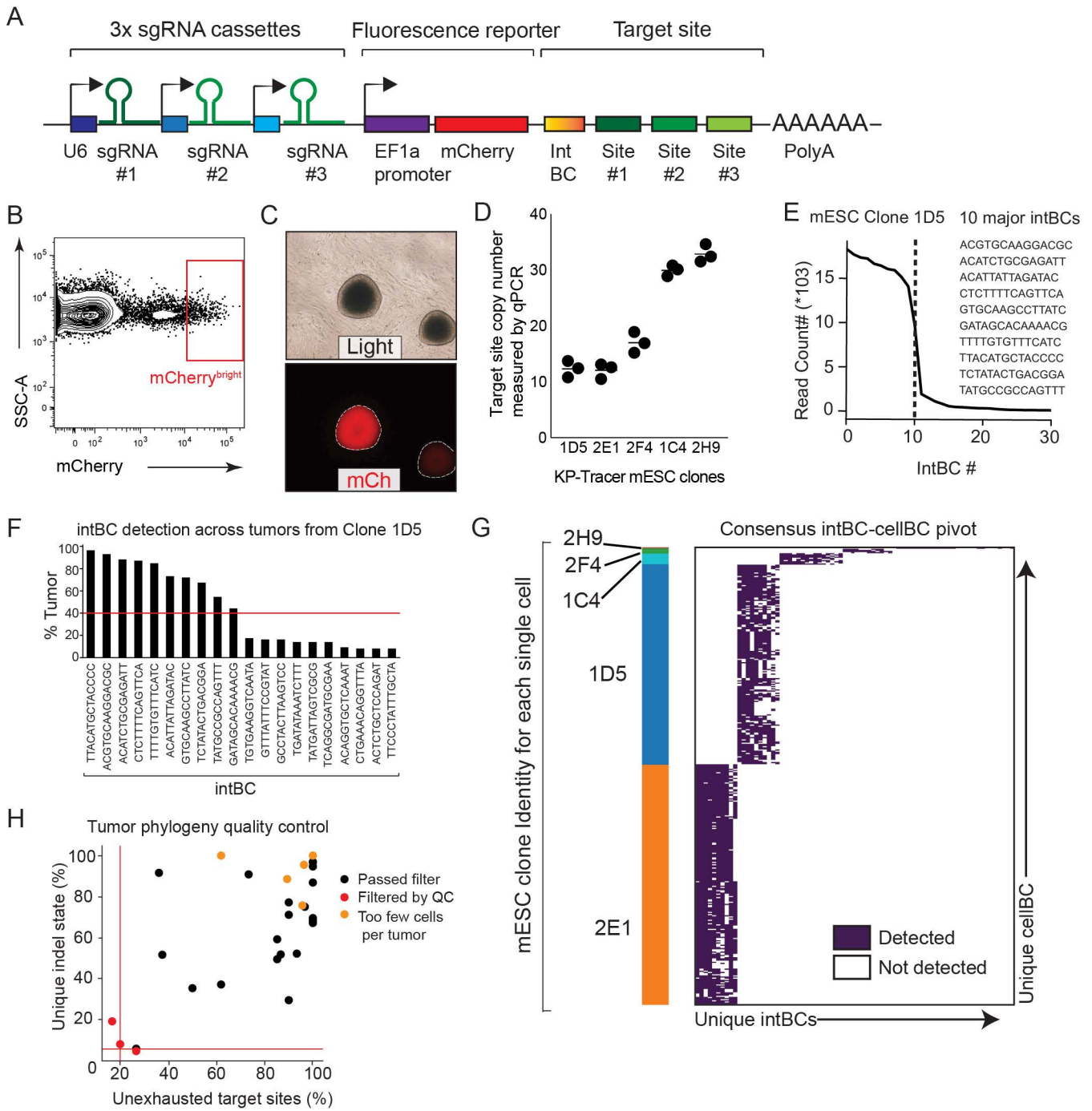


## **SUPPLEMENTARY MATERIALS**

*Supplementary Figures, Legends and Tables.*



## Figure S1. KP-Tracer mouse genetic components, validation, and quality-control

(A) The piggyBac transposon-based lineage tracing vector libraries used to engineer the KP-Tracer mice contained (1) a triple-guideRNA cassette and (2) a target site library cassette with a 14bp integration barcode (“intBC”) and three CRISPR/Cas9 cut sites on the 3’ UTR of an mCherry reporter gene.

(B) Enrichment of mESC population with high lineage-tracer expression based on high mCherry expression (a reporter indicating lineage tracer expression). These cells are then single-cell cloned before generating chimeric KP-Tracer mice.

(C) Representative images of specific mCherry positive mESC clones that express the lineage tracing vectors.

(D) Copy number of lineage tracing vectors across 5 mouse embryonic stem cell (mESC) clones used in this study measured by genomic qPCR are shown.

(E-F) Detection of unique lineage tracing target site intBCs for a representative mESC clone (1D5) using (E) DNA-sequencing and (F) scRNA-seq. A consensus set of target sites intBCs for each mESC clone was determined by selecting intBCs detected in at least 40% of all tumors derived from that mESC clone.

(G) The consensus intBC pivot table across all five mESC clones used in this study to generate KP-Tracer mice. Each row is a single cell and is annotated with which mESC clone it came from. Each column is a unique intBC. Colors in the heatmap indicate whether or not an intBC was detected in a given cell.

(H) Quality-control filtering of tumor phylogenies for subclonal expansion analyses. Quality of lineage-tracing data was assessed with two metrics: first, the percentage of cells that contained a unique set of mutations (“% unique indel state”; STAR Methods); and second, the percentage of target sites that had to be filtered because of low-diversity (“target site saturation”; STAR Methods). Tumors with less than 5% overall unique indel state, greater than 80% target site saturation, or fewer than 100 cells were filtered out.

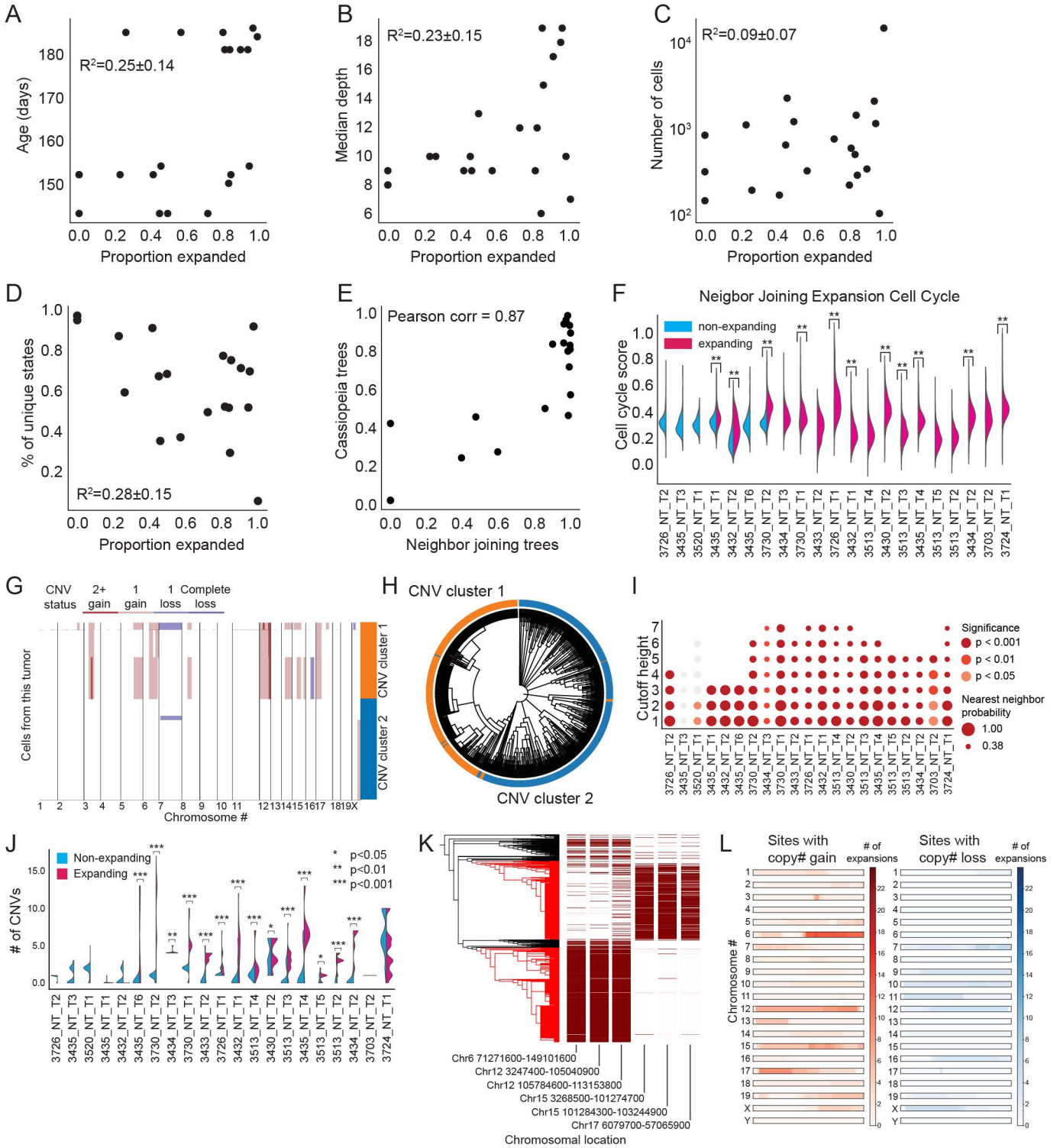


## Figure S2. Characterization of tumor subclonal expansions

(A-D) Phylogenetic features of tumor lineages and their predictiveness (as measured with  $R^2$ ) on the expansion proportion of a tumor. Features evaluated were (A) age, (B) median tree depth, (C) size measured in the number of cells, and (D) proportion of unique cells.

(E) Expansion proportion of tumors measured from Neighbor-Joining trees versus Cassiopeia trees. The percentage of cells in expansions were highly consistent between these two tree reconstruction strategies (Pearson's correlation = 0.87).

(F) Comparison of cell-cycle scores inferred from transcriptomic profiles in expanding versus non-expanding tumor subclones, identified from Neighbor-Joining trees (\*\*  $p < 0.01$ ).

(G-H) Representative example of comparison between hierarchical clustering of CNVs and Cassiopeia-reconstructed phylogeny. (G) The inferred CNVs are shown for the representative tumor, with the largest two clusters, identified via hierarchical clustering, indicated by the colorbar. (H) These two clusters are also indicated with unique colors on the Cassiopeia-reconstructed tumor phylogeny. The good correlation between CNV status and tumor phylogeny indicates the accuracy of tree reconstruction.

(I) Heatmap displaying the probabilities that a cell and its nearest neighbor on the Cassiopeia-reconstructed phylogeny are in the same CNV cluster (size of circles). These probabilities were calculated for each tumor at various depths of the CNV hierarchical clustering dendrogram. The depth that yielded the most coarse-grained clusters were set to have a cutoff height of 1, with higher cutoff heights indicating finer clusters. The majority of Cassiopeia-reconstructed phylogenies were significantly consistent with CNV clusters (color of circles; Permutation Test) at all clustering resolutions.

(J) A comparison of CNV counts in expanding versus non-expanding portions of tumors (\*  $p < 0.05$ , \*\*  $p < 0.01$ , \*\*\*  $p < 0.001$ ).

(K) An example of distinct CNV regions of cells from a single tumor. This tumor underwent two independent clonal expansions (red branches; left), each of which exhibited distinct CNV patterns (red bars; right).

(L) An aggregated view of the CNV "hotspots" across subclonal expansions from all tumors. Each horizontal bar represents a chromosome, and the intensity of color indicates the number of subclonal expansions exhibiting a CNV in a region (see Methods). Regions that more often exhibited copy number gains are indicated in red (left); genomic regions that more often exhibited copy number losses are indicated in blue (right).

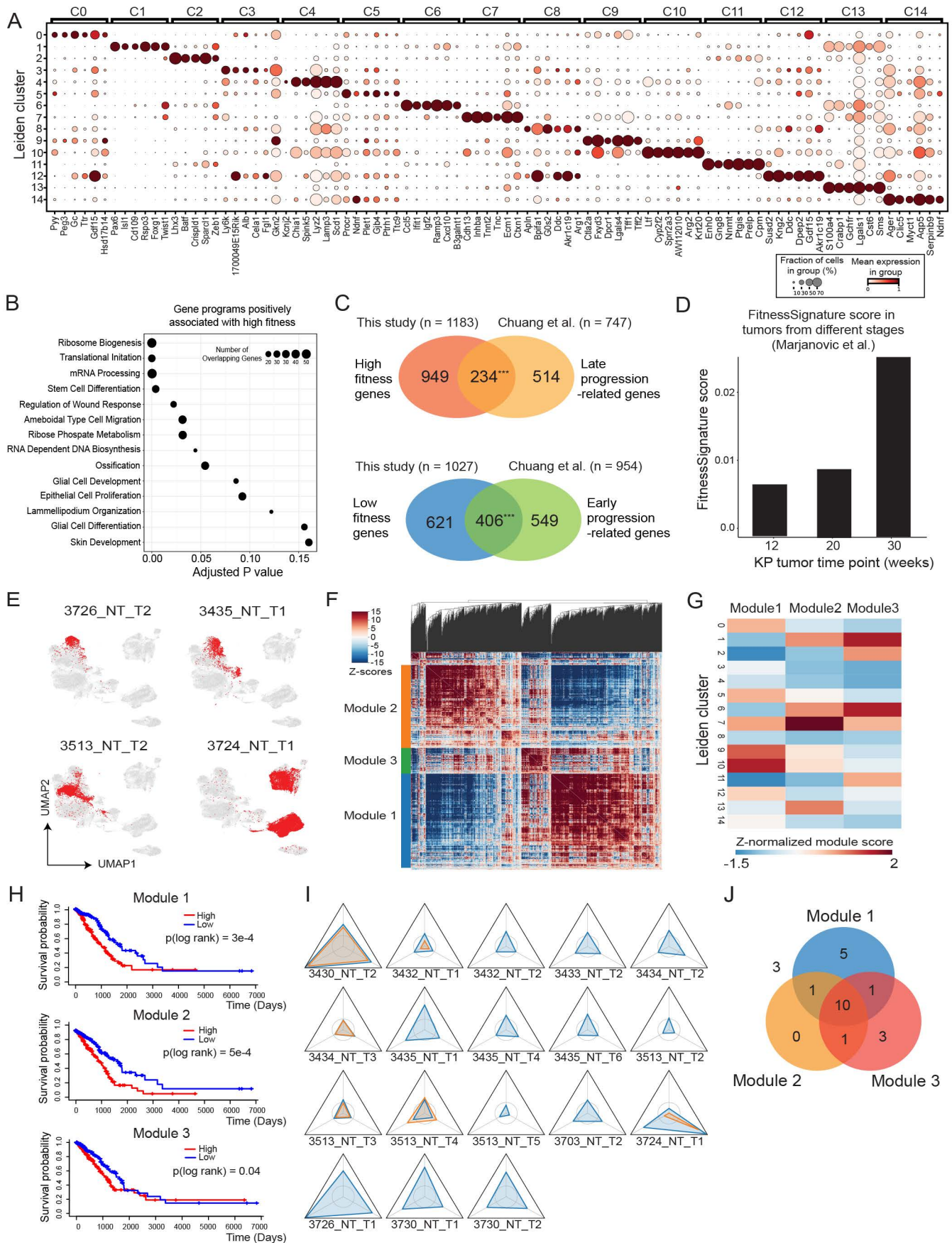


### Figure S3. Characterization of transcriptomic fitness landscape

(A) Gene markers for each Leiden cluster identified in the processed scRNA-seq latent space. Dot size indicates the percent of cells expressing the marker. Color indicates mean expression level.

(B) Gene set enrichment analysis of genes associated with high fitness using the biological process (BP) gene sets. Selected sets passing an FDR cutoff of 0.2 are shown. Dot size indicates the number of genes that appear in the gene set of interest.

(C) Gene set comparison between the FitnessSignature described in this study and KP tumor progression-associated genes described in (Chuang et al., 2017). Overlap significance assessed with a hypergeometric test ( $*** = p < 1e-5$ ).

(D) Average transcriptional FitnessSignature score in KP tumors harvested at 12-week, 20-week, and 30-week timepoints from (Marjanovic et al., 2020).

(E) Representative examples of tumors occupying distinct regions of the transcriptional space. Cells from the tumor of interest are shown in red, and all other cells are shown in gray.

(F) *Hotspot* autocorrelation heatmap and clustering of genes that appear in the FitnessSignature and are positively associated with fitness. Gene modules are identified by distinct color strips on the left. Values in the heatmap are *Z*-normalized pairwise autocorrelation scores between genes. The dendrogram linking genes is shown for the columns.

(G) *Z*-normalized mean fitness gene module signature scores of each Leiden cluster.

(H) Kaplan-Meier plots for TCGA human lung adenocarcinoma patients with respect to genes in each fitness module. Curves are shown comparing overall survival of patient groups whose tumors have high (red) versus low (blue) expression of individual fitness gene modules, as determined by the median fitness module score. P-values from a log-rank test are indicated.

(I) Fitness module enrichment personality plots. Each corner of the triangle represents the fold enrichment of an expansion's fitness module expression over expectation (non-expanding background). Independent expansions in each tumor are shown in unique colors (blue or orange).

(J) Venn diagram illustrating the classification of expansions to gene modules based on a p-value threshold of 0.05 using a permutation test against non-expanding background.

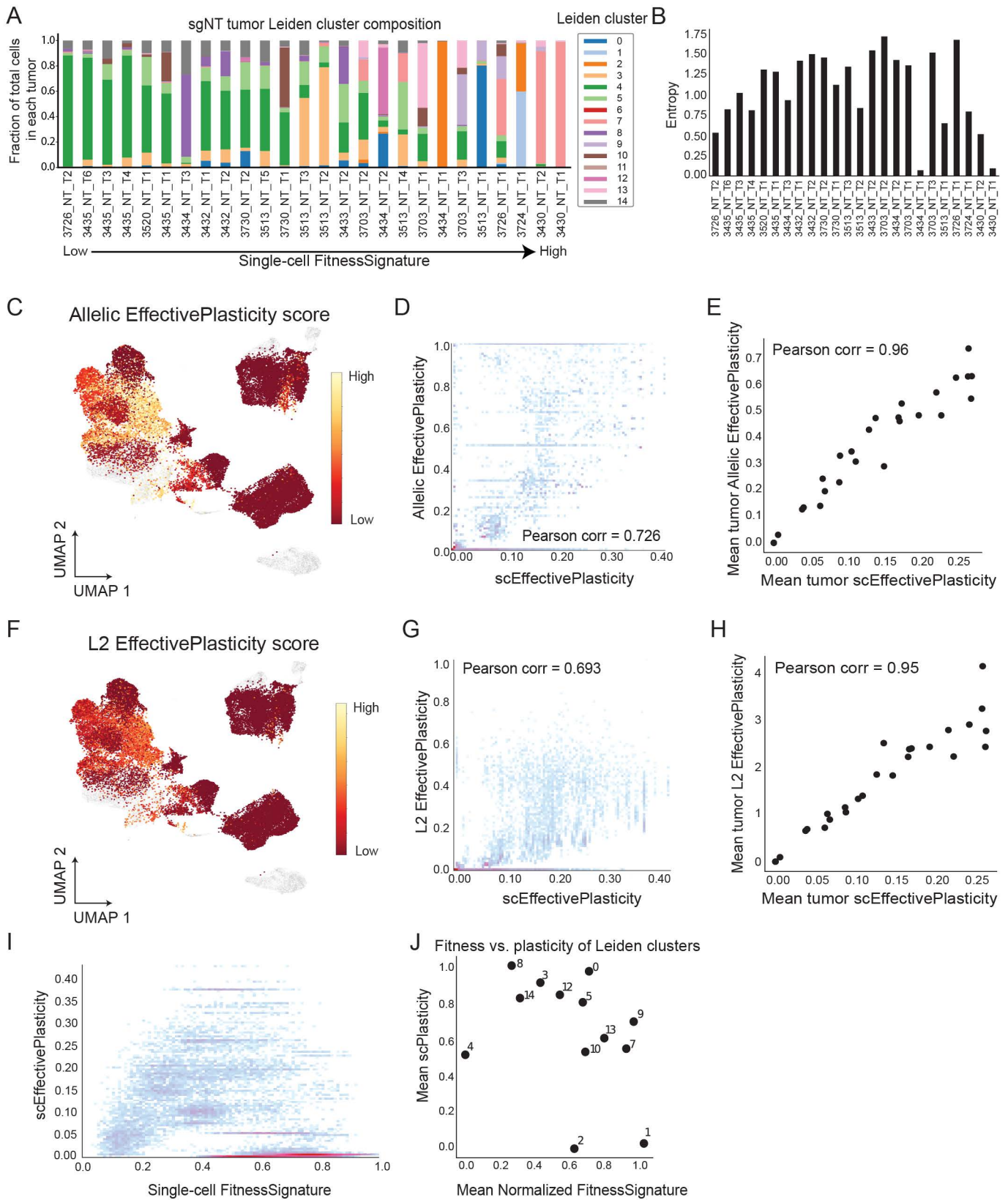


## Figure S4. Validation of EffectivePlasticity score and comparison to FitnessSignature

(A) Leiden cluster proportions for each KP-Tracer tumor. The fraction of cells in each Leiden cluster is shown for each tumor in a stacked bar plot, where each Leiden cluster is indicated by the unique color introduced in Fig 3A. Tumors are ordered by mean FitnessSignature score.

(B) Shannon's Entropy statistic for each tumor, computed with the Leiden cluster proportions; tumors are ordered by mean FitnessSignature score.

(C) Allelic EffectivePlasticity score overlaid onto two-dimensional gene expression UMAP is shown. Allelic EffectivePlasticity is an alternative way to quantify EffectivePlasticity by comparing transcriptional states between cells with similar lineage tracing indel states without using lineage trees.

(D) Comparison of Allelic EffectivePlasticity to scEffectivePlasticity (Pearson's correlation = 0.73). Each point represents a single cell.

(E) Comparison of mean tumor Allelic EffectivePlasticity to tumor EffectivePlasticity (Pearson's correlation = 0.96). Each point represents a tumor.

(F) L2 EffectivePlasticity score overlaid onto two-dimensional gene expression UMAP is shown. L2 EffectivePlasticity is another alternative way to quantify EffectivePlasticity by computing dissimilarity in gene expression profiles between nearest neighbors on the phylogeny.

(G) Comparison of single-cell L2 EffectivePlasticity to scEffectivePlasticity (Pearson's correlation = 0.69). Each point represents a single cell.

(H) Comparison of mean tumor L2 EffectivePlasticity to mean tumor EffectivePlasticity (Pearson's correlation = 0.95). Each point represents a tumor.

(I) Comparison of scEffectivePlasticity to single-cell FitnessSignature scores. Each point represents a single cell.

(J) Weighted mean EffectivePlasticity vs mean FitnessSignature for each transcriptional state (Leiden cluster). The weighted Mean EffectivePlasticity for each Leiden cluster was determined by first computing the mean scEffectivePlasticity for each Leiden cluster in a tumor, and then averaging these values together. Each point represents a tumor.

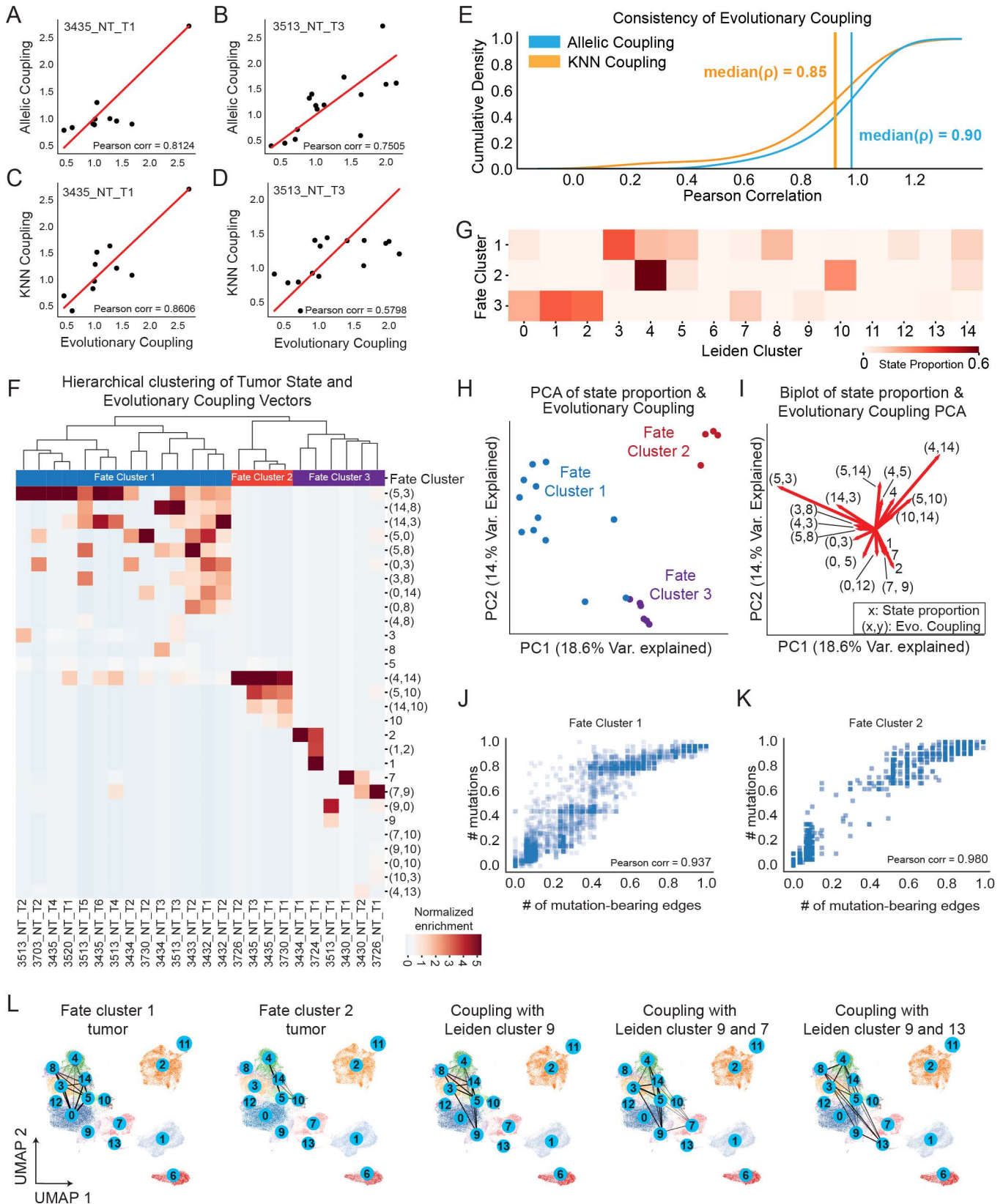


## Figure S5. Validation of Evolutionary Coupling and Fate clustering

(A-D) Two alternative statistics measuring couplings between states from lineage tracing data are used to corroborate the Evolutionary Coupling results for the representative tumors 3435\_NT\_T1 and 3513\_NT\_T3 shown in Figure 5 A-D. The comparisons between Allelic Coupling and Evolutionary Coupling for (A) 3435\_NT\_T1 and (B) 3513\_NT\_T3 are consistent (Pearson's correlation = 0.94 and 0.99, respectively). The comparisons between KNN Coupling and Evolutionary Coupling for (C) 3435\_NT\_T1 and (D) 3513\_NT\_T3 are consistent (Pearson's correlation = 0.97 and 0.86, respectively). Red line indicates the symmetrical  $y=x$  relationship.

(E) Cumulative density function for Pearson's correlation of Allelic Coupling and KNN Coupling statistics with Evolutionary Couplings for all KP-Tracer tumors. Median correlations are indicated with vertical bars and annotated with the median correlation value.

(F) Clustering of tumors based on Evolutionary Coupling and Leiden cluster proportion statistics reveals features that distinguish different Fate Clusters. Three clusters are identified by unbiased clustering, corresponding to Fate Clusters 1, 2, and 3. Fate Cluster is annotated on top of each unique color in the first row of the heatmap. Values/colors in the heatmap are normalized across tumors, and each row corresponds to a feature (either an Evolutionary Coupling or Leiden cluster proportion). Evolutionary couplings are indicated by a tuple of the form  $(x, y)$  and Leiden cluster proportions are indicated by a single number of the form  $x$ . We focus on showing features that distinguish different clusters, and uninformative features, identified as non-significant by a Mann-Whitney U test ( $p > 0.1$ ), are not shown.

(G) Heatmap of state proportions for each Fate Cluster across Leiden clusters. The value of the  $i^{\text{th}}$  row and  $j^{\text{th}}$  column indicate the fraction of cells found in the  $j^{\text{th}}$  Leiden Cluster across all tumors in the  $i^{\text{th}}$  Fate Cluster.

(H) Principal Component Analysis (PCA) of tumor Evolutionary Coupling and Leiden cluster proportion vectors. Each dot is a tumor. Tumors are colored by their Fate Cluster, as identified with the hierarchical clustering shown in Fig S5E. The percent of variance explained is indicated on each axis.

(I) Biplot of PCA of Evolutionary Coupling and Leiden cluster composition vectors, where each arrow indicates the loading of the feature with respect to the first two principal components. The top 10 features for the first two principal components are shown; arrows are annotated with the feature label. The percent of variance explained is indicated on each axis. Features of the form  $(x, y)$  represent Evolutionary Couplings between state  $x$  and state  $y$ ; features of the form  $x$  represent the proportion of cells found in Leiden cluster  $x$ .

(J-K) Comparison of Phylotime statistics computed using weighted and binary tree branch lengths for (J) Fate Cluster 1 and (K) Fate Cluster 2 (STAR Methods). Correlations are strong for both Fate Clusters (Pearson's correlation = 0.94 and correlation = 0.98, respectively).

(L) Selected Evolutionary Couplings of individual tumors displayed on gene expression UMAP illustrating connections between transcriptional states (Leiden clusters) of interest. From left: the

first plot shows the Evolutionary Couplings within a representative tumor in Fate Cluster 1. The second plot shows the Evolutionary Couplings within a representative tumor in Fate Cluster 2. The third plot shows couplings between Fate Cluster 1 (Leiden clusters 3 and 5) and Late stage transcriptome states (Leiden cluster 9). The fourth plot shows couplings between Fate Cluster 1 (Leiden clusters 3 and 5) and high fitness transcriptome states (Leiden cluster 7 and 9). The last plot shows couplings between Fate Cluster 1 (Leiden clusters 3, 5 and 14) and high fitness transcriptome states (Leiden cluster 9 and 13). These results offer evidence of potential transition from early, low fitness to late, high fitness transcriptome states during tumor evolution.

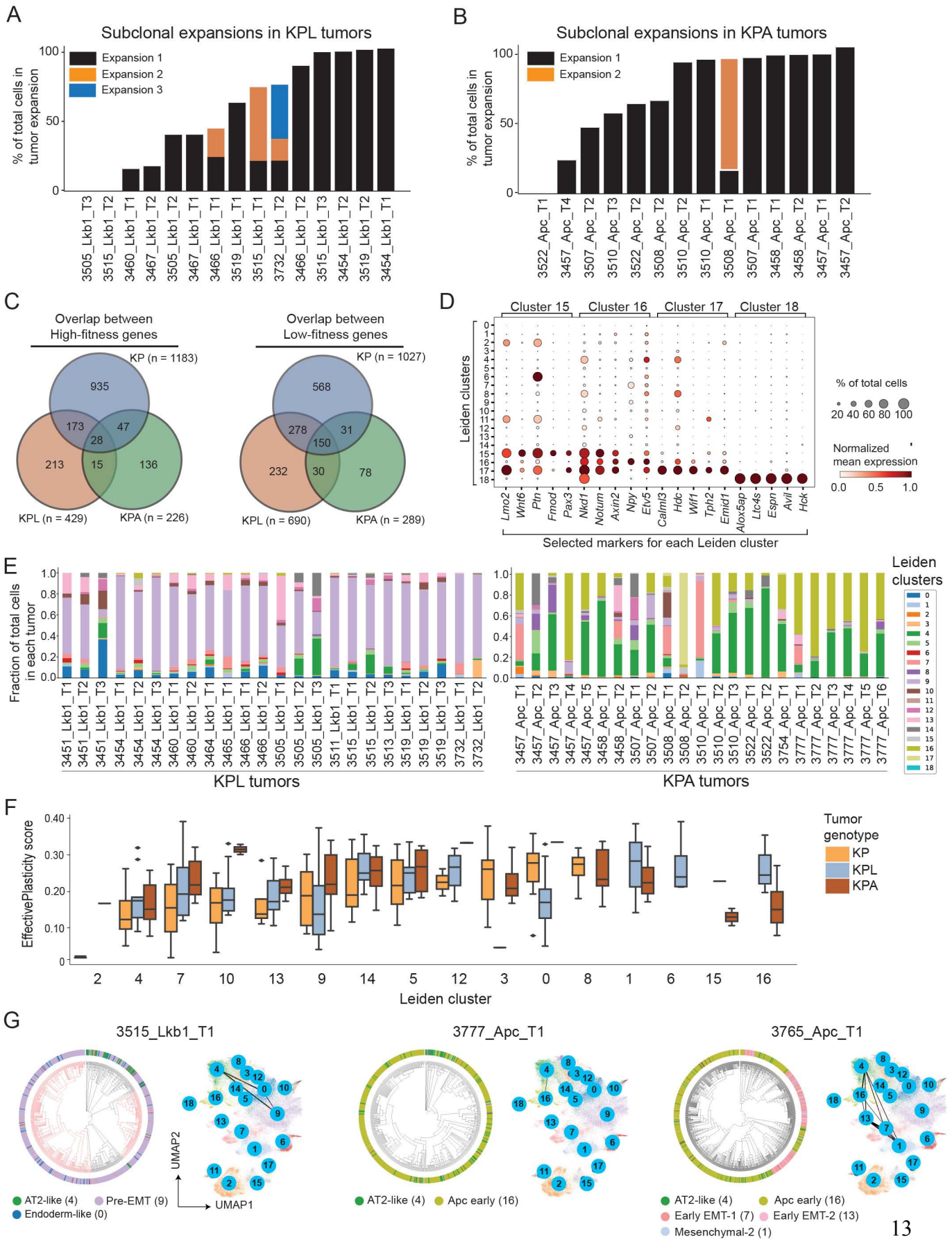


## Figure S6. Genetic perturbations shift the transcriptional fitness and plasticity landscape of tumors

(A-B) Subclonal expansion dynamics of (A) KPL and (B) KPA tumors. Independent expansions are colored with black, orange or blue and measured with the percentage of cells in the expanding subclone.

(C) Overlap of genes associated with high and low fitness for KP, KPL and KPA tumors.

(D) Gene markers for newly identified Leiden clusters in the KP, KPL and KPA integrated analysis. Dots are sized by the fraction of cells expressing a marker and colored by the mean expression of the gene marker in a Leiden cluster.

(E) Leiden cluster proportions for each KPL (left) and KPA (right) tumor.

(F) Distribution of the mean EffectivePlasticity for each Leiden cluster, averaged within each tumor, compared across genotypes. Leiden clusters 6, 11, 17, 18 are not shown because they lacked enough tumors across genotypes to make comparisons.

(G) Evolutionary Couplings of different transcriptional states in three representative tumors reveals evolutionary paths in KPL and KPA tumors. Transcriptional states that are represented by at least 2.5% of cells in each tumor are used. 3515\_Lkb1\_T1 is a representative KPL tumor. The left plot shows the lineage relationship of transcriptional states in this KPL tumor and the right plot summarizes Evolutionary Couplings on the gene expression UMAP illustrating connections between Leiden clusters 4, 0 and 9. 3777\_Apc\_T1 is a representative KPA tumor. The left plot shows the lineage relationship of transcriptional states in this KPL tumor and the right plot summarizes Evolutionary Couplings on the gene expression UMAP illustrating connections between Leiden clusters 4 and 16. 3765\_Apc\_T1 is another representative KPA tumor. The left plot shows the lineage relationship of transcriptional states in this KPL tumor and the right plot summarizes Evolutionary Couplings on the gene expression UMAP illustrating connections between Leiden clusters 4, 16, 13, 7 and 1.

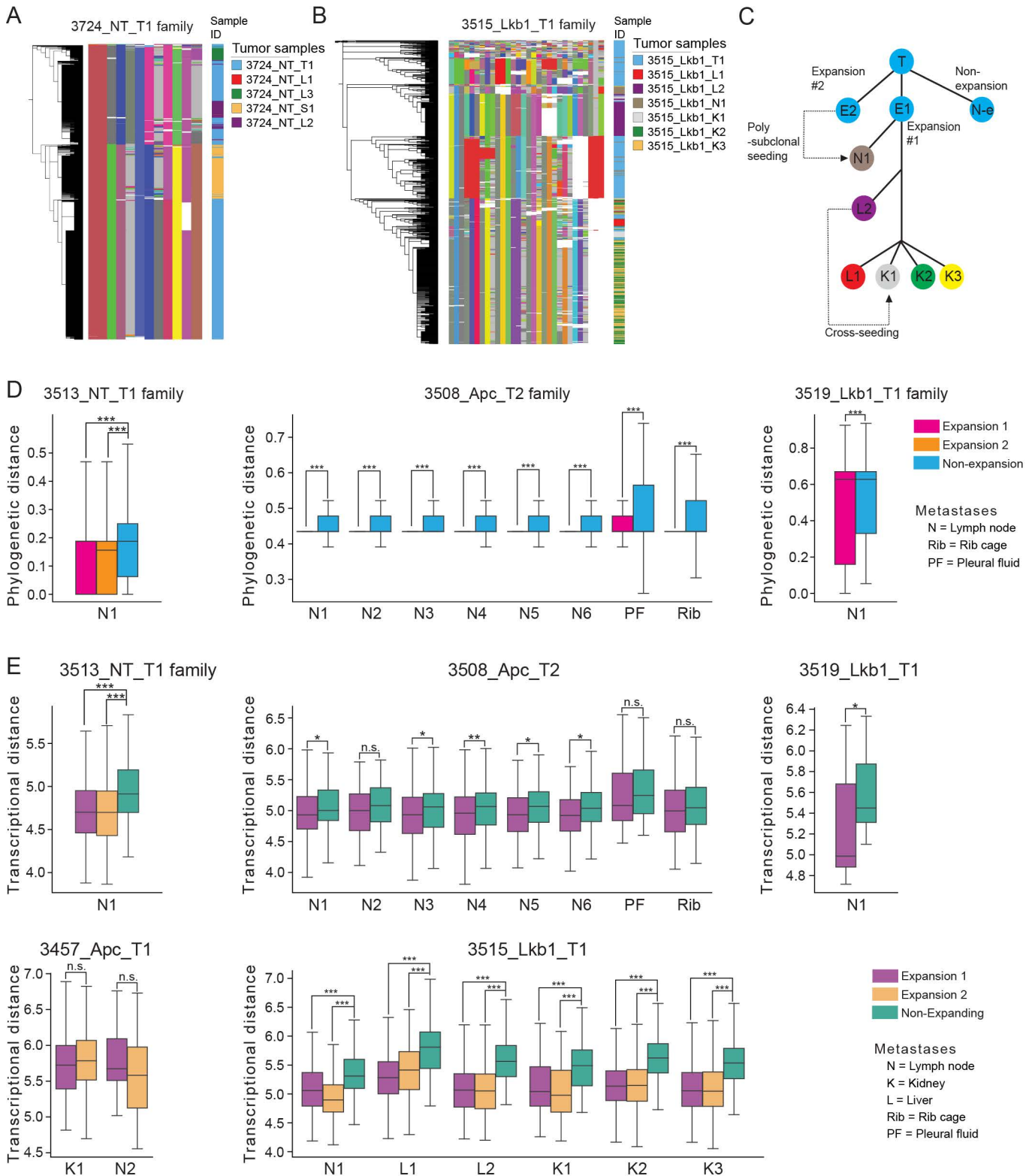


### Figure S7. Lineage tracing illuminates the metastatic routes and origins

(A) Lineage indel heatmap of the 3724\_NT\_T1 tumor-metastasis family, summarizing the allelic information (indels) from the target sites confirming the separate origin of the soft tissue and liver metastatic tumors. In the Lineage indel heatmap, each row represents a single cell and each column represents a cut site of the lineage tracer. Unique indels are shown in unique colors, uncut target sites are indicated in gray, and missing data is indicated in white. The reconstructed lineage based on the accumulated indel patterns using Cassiopeia are shown on the left. The corresponding sample ID for each cell is labeled on the right.

(B-C) Subclonal origin and the metastatic routes for 3515\_Lkb1\_T1 tumor-metastasis family. (B) Lineage indel heatmap of 3515\_Lkb1\_T1 tumor-metastasis family, indicating indel alleles supporting the subclonal origins, the relative order and the routes of metastases and (C) a model summarizing these metastatic behaviors.

(D) More supporting examples of expanding subclones giving rise to metastases across genotypes for 3513\_NT\_T1 (left), 3508\_Apc\_T2 (center), and 3519\_Lkb1\_T1 (right).

(E) Comparison of transcriptional distance between metastatic tumors and cells in non-expanding and expanding regions of the primary tumor phylogeny for 3513\_NT\_T1, 3508\_Apc\_T2, 3519\_Lkb1\_T1, 3457\_Apc\_T1, and 3515\_Lkb1\_T1 metastasis families. All significances are indicated from a one-sided Mann-Whitney U test: \*\*\* indicates  $p < 0.001$ , \*\* indicates  $p < 0.01$ , and \* indicates  $p < 0.05$ .